# Volume and surface propellant heating in an electrothermal radio-frequency plasma micro-thruster

A. Greig, C. Charles, N. Paulin, and R. W. Boswell

**Articles you may be interested in**

Direct measurement of neutral gas heating in a radio-frequency electrothermal plasma micro-thruster
Appl. Phys. Lett. **103**, 074101 (2013); 10.1063/1.4818657

Microwave-excited microplasma thruster with helium and hydrogen propellants
Phys. Plasmas **18**, 063505 (2011); 10.1063/1.3596539

Characterization of a radio frequency carbon nanotube growth plasma by ultraviolet absorption and optical emission spectroscopy
J. Appl. Phys. **97**, 084311 (2005); 10.1063/1.1865315

Measurements and modeling of ion and neutral distribution functions in a partially ionized magnetically confined argon plasma
Phys. Plasmas **11**, 4008 (2004); 10.1063/1.1768175

Enhancement of ion extraction from a cold plasma with radio-frequency plasma heating
Appl. Phys. Lett. **76**, 1822 (2000); 10.1063/1.126177

# Volume and surface propellant heating in an electrothermal radio-frequency plasma micro-thruster

A. Greig,[a)] C. Charles, N. Paulin,[b)] and R. W. Boswell

*Space Plasma, Power and Propulsion Laboratory, Research School of Physics and Engineering, The Australian National University, Canberra, Australian Capital Territory 0200, Australia*

The temporal evolution of neutral gas temperature over the first 5 min of operation for an electrothermal radio-frequency micro-thruster with nitrogen ($N_2$) propellant was measured using rovibrational band matching of the second positive $N_2$ system. Three distinct periods of gas heating were identified with time constants of $\tau_1 = 8 \times 10^{-5}$ s, $\tau_2 = 8$ s, and $\tau_3 = 100$ s. The fast heating ($\tau_1$) is attributed to volumetric heating processes within the discharge driven by ion-neutral collisions. The slow heating ($\tau_3$) is from ion neutralization and vibrational de-excitation on the walls creating wall heating. The intermediate heating mechanism ($\tau_2$) is yet to be fully identified although some theories are suggested. © 2014 AIP Publishing LLC. [http://dx.doi.org/10.1063/1.4892656]

Micro-propulsion devices designed for micro- or nano-satellite operation need to be small, lightweight, and low power and can be chemical, electromagnetic, or electrothermal.[1–4] The simplest micro-propulsion device, the cold gas thruster, expels an inert gas through a nozzle to produce thrust,[2] but efficiency is low as the gas emitted is cold. Increased efficiency may be achieved by heating the gas through electrical or other means. An electrothermal plasma micro-thruster under development at The Australian National University is the pocket rocket device, previously fully described,[5,6] and shown in Figure 1. The device operates on a few tens of Watts of radio-frequency (rf) (13.56 MHz) power creating a capacitively coupled plasma discharge inside a 20 mm long, 4.2 mm diameter alumina tube. Gas is introduced through an upstream plenum chamber that contains a viewport to allow optical and probe diagnostics of the plasma volume.

Recent computational fluid dynamics simulations of the thruster show that the primary ionization mechanism is through secondary electrons from ion bombardment of the alumina tube surfaces,[7] creating a peak in plasma density in the center of the tube which has been observed experimentally.[6] The steady state neutral gas temperature ($T_g$) within the pocket rocket discharge was previously measured for steady state continuous operation in nitrogen ($N_2$) and argon with 1% $N_2$ using rovibrational spectroscopy.[8] For 10 W power input, the argon (with 1% $N_2$) discharge gave $T_g \approx 1100$ K while the $N_2$ discharge gave $T_g \approx 430$ K.

Gas heating mechanisms within plasma discharges include both volume and surface effects.[9–16] Volume heating results from energy being redistributed between the electronic, translational, rotational, and vibrational states through elastic collisions,[9,16] ion-neutral charge exchange collisions,[10,11,15] quenching,[12,13] dissociation, and vibration-vibration (V-V) and vibration-translation (V-T) relaxation.[12,16] Surface or wall heating results from a mechanism, such as ion neutralization,[14]

metastable quenching,[12,16] or vibrational de-excitation,[12,16] through collisions with the walls, which transfers energy to the surface increasing the temperature of the walls, which then transfers energy into the neutral gas through convection and conduction processes.

Here, the temporal evolution of temperature in a 1.5 Torr, 60 W, $N_2$ discharge was recorded and analyzed to determine the heating time constants within the pocket rocket device, from which the bulk heating methods were estimated. The rotational ($T_r$) and vibrational ($T_v$) temperatures were measured using rovibrational band matching of the second positive system of $N_2$[17] with $T_g \approx T_r$ at pressure around a Torr.[13] This is the same method as described previously to determine the steady state temperatures in pocket rocket.[8]

To control the time each experimental rovibrational spectrum was recorded, a specially written Labview program simultaneously controlled the rf power generator used to generate the plasma and charge coupled device (ccd) array used to capture the spectra, to synchronize the initiation and
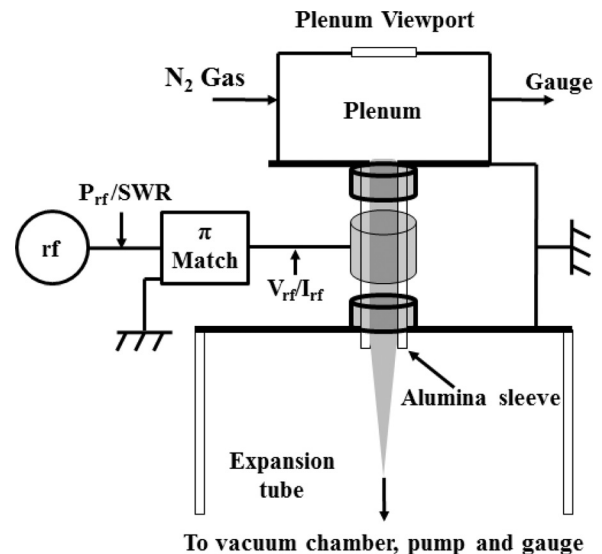


FIG. 1. The pocket rocket device.

duration of the plasma discharge with the integration timing of the ccd array. To allow a temporal evolution capturing seven orders of magnitude, from 50 $\mu$s to 300 s, two different timing techniques were required. For the 50 $\mu$s to 20 ms time range, the thruster was pulsed at the duration of interest while the ccd array integrated continuously for 500 ms, capturing light output from multiple pulses of the discharge. This was necessary to capture the short time scales as light intensity from a single pulse of these durations gave insufficient rovibrational spectra signals for matching. The integration time of 500 ms was chosen arbitrarily as a value where enough light from multiple pulses had accumulated to provide a strong rovibrational spectra signal. A 2.5% duty cycle ensured no residual heat was left in the system between pulses. For the 50 ms–300 s time range, the thruster was operated in continuous mode for 300 s, while the ccd array recorded 8 ms integrations at 168 set times, with the procedure repeated 12 times averaging the recorded spectra to reduce the effect of noise.

Results for the temporal evolution of $T_r$ and $T_v$ in a 1.5 Torr, 60 W, $N_2$ discharge are shown in Figure 2 using a log scale for time. The blue circles denote $T_r$ and are equivalent to $T_g$, with $T_v$ denoted by the red squares. A sharp increase in $T_r$ to ~420 K occurs within the first 200 $\mu$s, followed by a slower increase to the final measured temperature of 580 K at 300 s. These results are in agreement with the previous results that measured a steady state $N_2$ gas temperature of ~430 K for 10 W input power.[8] This experiment was performed at higher power (60 W) to give sufficient signal strength with shorter integration times, explaining the slightly higher temperature measured here. An increase in $T_v$ to ~3900 K occurs within 10 ms before remaining at a similar temperature for the remainder of the 300 s operation, with a possible slight decrease of ~100 K between 1 and 10 s.

Different heating or cooling mechanisms within the discharge occur on different timescales and hence can be separated and identified using the time constant ($\tau$) of the temperature change. Equations of the form $T = T_0 + \Delta T (1 - e^{-\frac{t}{\tau}})$ for heating and $T = T_0 + \Delta T e^{-\frac{t}{\tau}}$ for cooling, where $T_0$ is the initial temperature and $\Delta T$ is the total temperature change, were fitted to the data to estimate the time constants

of various heating and cooling periods. The equation for $T_v$ is given by Eq. (1) and is shown in Figure 2 as a solid red line overlayed on the experimental data. A temperature of 3395 K was chosen for $T_{v0}$ to match the characteristic vibrational temperature of $N_2$.[18] The equation for $T_r$ is given by Eq. (2) and is shown in Figure 2 as a solid blue line. Ambient temperature (300 K) was chosen for $T_{r0}$. Data points between 100 $\mu$s and 10 ms lie slightly below the fit curve, as the ccd array performed long integrations recording the entire pulse width, instead of a small window in continuous plasma operation as with the remaining points, slightly underestimating temperature

$$T_v = 3395 + 450\left(1 - e^{-\frac{t}{2\times10^{-4}}}\right) + 100\left(e^{-\frac{t}{8}}\right), \qquad (1)$$

$$T_r = 300 + 140\left(1 - e^{-\frac{t}{8\times10^{-5}}}\right) + 100\left(1 - e^{-\frac{t}{8}}\right) + 60\left(1 - e^{-\frac{t}{100}}\right). \qquad (2)$$

Vibrational temperature evolution exhibits one heating period with $\Delta T_{v1} = +450$ K and $\tau_{v1} = 2 \times 10^{-4}$ s or 200 $\mu$s and one cooling region $\Delta T_{v2} = -100$ K and $\tau_{v2} = 8$ s. The heating is most likely due to electron impact excitation of vibrational states. The cooling is possibly due to V-V and V-T relaxation, supported by a corresponding increase in $T_r$ of 100 K with $\tau_{r2} = 8$ s, suggesting there is a transfer of energy from vibrational to translational states. As the rotational and translational states are assumed to be in equilibrium, a change in energy of the translational states will be evident in the rotational states and hence $T_r$.

The vibrational relaxation time of simple systems can be reasonably estimated using the following equation:[18]

$$\ln(p\tau_v) = (1.16 \times 10^{-3})\mu^{\frac{1}{2}}\theta^{\frac{4}{3}}\left(T^{-\frac{1}{3}} - 0.015\mu^{\frac{1}{4}}\right) - 18.42, \quad (3)$$

where $T$ is in Kelvin, p is the pressure in atmospheres, $\mu$ is the reduced mass of the molecule ($\mu = 14$ for $N_2$), and $\theta$ is the characteristic vibrational temperature. Using Eq. (3), a vibrational relaxation time constant of $\tau_v = 8$ s is found for a temperature of ~1150 K. This is just over twice the measured temperature at that time of ~550 K. However, the empirical method only claims 50% accuracy of the actual value for temperatures between 300 K and 8000 K based on correlation with experimental results.[18] It is therefore possible the apparent exchange of energy from vibrational to rotational here is due to vibrational relaxation but further testing beyond the scope of this study is required to confirm this hypothesis.

Rotational temperature, hence neutral gas temperature, also exhibits two other heating periods, the first with $\Delta T_{r1} = 140$ K with $\tau_{r1} = 8 \times 10^{-5}$ s or 80 $\mu$s, the other with $\Delta T_{r3} = 60$ K with $\tau_{r3} = 100$ s. The rise time of the rf generator is around 70 $\mu$s with plasma breakdown occurring approximately 45 $\mu$s into the rf pulse as seen in Figure 3, showing the normalized rf voltage envelope during an 800 ms pulse measured at a location after the matching network (panel (a)), corresponding photodiode signal of discharge light emission (panel (b)) and ion saturation current measured with a Langmuir Probe (LP) (panel (c)). The LP was inserted through the rear plenum viewport such that the
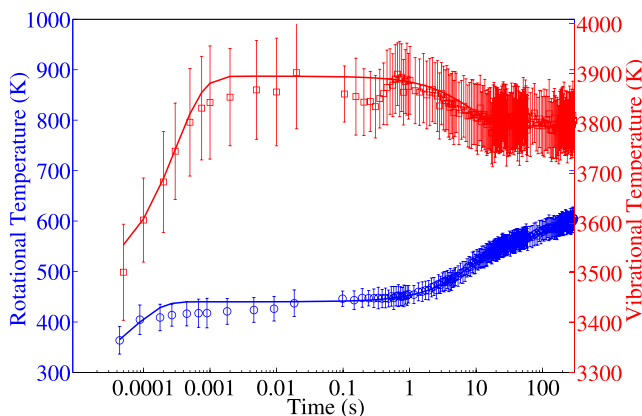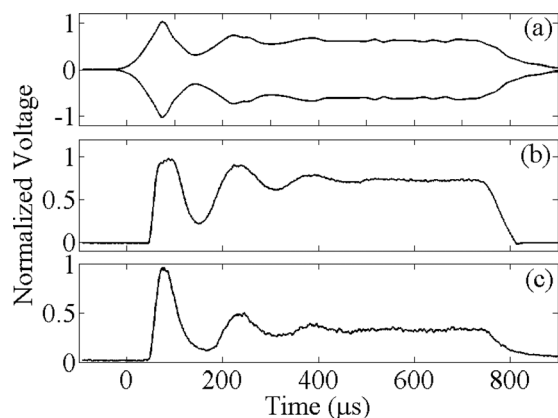


FIG. 2. Temporal evolution of $T_r$ (blue circles) and $T_v$ (red squares) time for a 1.5 Torr, 60 W, $N_2$ discharge. The solid lines show a fit equation to determine time constants, given by Eqs. (1) and (2) for vibration and rotation, respectively.

FIG. 3. Breakdown in the pocket rocket device during an 800 $\mu$s pulse showing (a) normalized rf voltage envelope post match, (b) normalized photodiode signal of discharge light emission, and (c) normalized ion saturation current measured with a Langmuir probe.

1 mm circular flat tip biased at $-29$ V was positioned on the central axis of the discharge tube, halfway down the length. Thus, the fast initial increase in $T_r$ occurs on the same timescale as the rise time of the rf generator and is likely caused by elastic and ion-neutral charge exchange collisions within the discharge, occurring on timescales at or below that of the rf generator rise time. This is approximately three times faster than the initial fast increase in $T_v$ from electron impact vibrational excitation. The cross section for ion-neutral charge exchange collisions[19] between $N_2^+$ and $N_2$ is around $10^{-14}$ cm$^2$ and the cross section for vibrational excitation of $N_2$ by electron impact[20] is around $10^{-20}$ cm$^2$; therefore, the collision frequency of ion-neutral charge exchange collisions will be higher than that for vibrational excitation by electron impact and the resulting heating will occur faster.

The slow rotational heating with $\tau_{r3} = 100$ s is most probably from ion neutralization and vibrational de-excitation through collisions with the walls, transferring energy into the alumina tube and increasing the wall temperature. Heat is then transferred back into the neutral gas through conduction and convection causing an increase in $T_g$, representative of the slow increase in $T_r$. A similar increase on these time scales is not seen for $T_v$, as vibrational states are excited through electron collisions and not through collisions with the walls.

To confirm if heating of the gas with $\tau = 100$ s from wall heating is feasible, a simple thermal model representative of the pocket rocket mechanical assembly was developed. The mechanical assembly was been decomposed into three isothermal volumes or thermal nodes: node 1 representing the inner alumina tube surface receiving heat Q from the plasma, node 2 representing an average temperature of the copper rf electrode, Macor (machinable glass-ceramic) electrode insulation and aluminum housing structure, and node 3 representing the aluminum outer surface of the housing and is considered a thermal sink at 313 K (40 °C), the temperature of the outer surface measured during the experiment. The initial temperature conditions were set to ambient (300 K) at nodes 1 and 2 and 313 K at node 3 (the thermal sink).

The thermal resistance between nodes 2 and 3, $R_{23} = 7.4 \times 10^{-2}$ K/W, was determined by the conductive thermal path in the cylindrical aluminum body using $R_{23} = \frac{\ln(r_2/r_1)}{2\pi kL}$,

where $r_2$ is the outside radius (36 mm), $r_1$ is the inner diameter (3.0 mm), $L$ is the length (30 mm), and $k$ is the thermal conductivity ($\sim$180 W/m·K for aluminum alloy). Thermal resistance between nodes 1 and 2 is more complex as it is determined by the thermal contact resistance at the interface between the different parts, which is dependant on contact pressure, surface roughness, and the nature and pressure of gas in the interstitial gap. Based on surface quality and low contact pressure, a poor conductance situation was assumed with a thermal conductance of 1000 W/m$^2$·K, giving a thermal resistance between nodes 1 and 2 of 7 K/W.

The heat transferred from the plasma to the surface of the alumina tube (Q) is from ion neutralization and vibrational de-excitation on the walls. Total power input to the system is 60 W with the matching networking having a measured efficiency of 67%, giving 40 W of power transferred into the plasma. The power carried out in the plasma plume is given by $P_{plume} = \frac{1}{2}\dot{m}v_{ex}^2 \approx 1$ W, where $\dot{m}$ is the flow rate (2.8 mg/s here) and $v_{ex}$ is the exhaust velocity estimated from the measured temperature of 600 K as 670 m/s using $v_{ex} = \left(\frac{8kT}{\pi M}\right)^{\frac{1}{2}}$ where M is the mass of an $N_2$ molecule. The remaining 39 W of power goes into ionization and excitation processes within the gas which is then assumed to be lost to the walls, giving Q = 39 W.

Results of the thermal simulation are shown in Figure 4, where the solid line represents the temperature of the inner alumina tube surface (node 1), the dashed line represents the average temperature of the housing structure (node 2), and the dotted line represents the temperature of the housing outer surface (node 3). The temperature on the alumina tube surface increases to 573 K after 300 s, similar to the experimental results of 580 K. To confirm if this result is consistent with the mechanical design of the pocket rocket system, the heat capacitance of the system (C) is calculated using $\tau_{model} = RC$, where $\tau_{model}$ is the time constant of the thermal model and $R$ is the total thermal resistance between the alumina and the thermal sink. From above, $R \approx 7$ K/W, and with $\tau = 100$ s, $C = \frac{100}{7} = 14$ J/K, which is not greater than the total heat capacitance (mass multiplied by specific heat capacity of the materials) of the aluminum, Macor and copper structures on the thermal path between node 1 and node
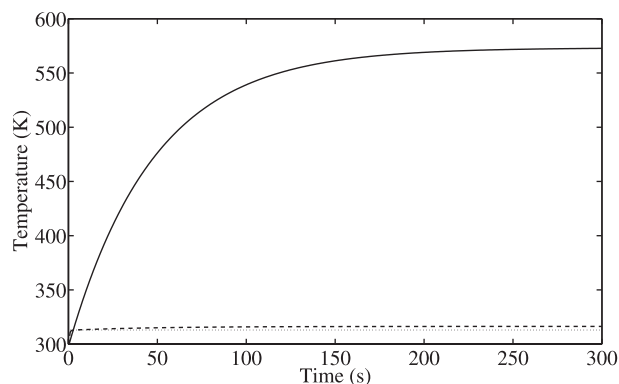


FIG. 4. Thermal model results for temperature of the alumina tube inner surface (solid line), average temperature of the housing structure (dashed line), and temperature of the outer housing skin (dotted line) with time for a 39 W power transfer to the alumina tube inner surface.

3, hence the thermal model is consistent with the mechanical design. These results confirm that ion neutralization and vibrational de-excitation of $N_2$ molecules on the alumina tube walls increase the wall temperature to around 573 K within a few hundred seconds, causing the neutral gas temperature to rise to nearly 600 K over similar time scales as observed experimentally.

The temporal evolution of $T_r$ and $T_v$ in the first 300 s of plasma operation in an electrothermal plasma micro-thruster has been measured using rovibrational spectroscopy for a 1.5 Torr, 60 W, $N_2$ discharge. Four heating and cooling mechanisms were identified: fast rotational heating with $\tau_{r1} = 80 \, \mu s$ from ion-neutral collisions within the plasma bulk; fast vibrational heating with $\tau_{v1} = 200 \, \mu s$ from electron impact excitation collisions, rotational heating and vibrational cooling, $\tau_{r2} = \tau_{v2} = 8$ s, possibly from energy transfer during vibration-translation relaxation processes; and slow rotational heating with $\tau_{r3} = 100$ s from wall heating caused by ion bombardment and vibrational de-excitation of $N_2$ with the alumina tube walls.

Neutral gas temperature is taken to be the same as rotational temperature as the pressure is sufficient for collisions to create equilibrium between rotational and translational states. Hence, there are three main heating mechanisms within the pocket rocket device acting to increase the temperature of the nitrogen gas (propellant) to approximately 580 K after 300 s of operation, being volume heating from ion-neutral charge exchange collisions, possible energy transferred to rotational and translational states through vibrational relaxation and wall heating from ion bombardment, and vibrational de-excitation collisions with the alumina tube walls.

[1]D. S. H. Charrier, Appl. Phys. Lett. **101**, 034104 (2012).
[2]J. Mueller, "Thruster options for microspacecraft," in *Micropropulsion for Small Spacecraft* (AIAA, 2000), pp. 45–137.
[3]M. Martinez-Sanchez and J. E. Pollard, J. Propul. Power **14**, 688 (1998).
[4]R. H. Frisbee, J. Propul. Power **19**, 1129 (2003).
[5]R. Boswell, C. Charles, P. Alexander, J. Dedrick, and K. Takahashi, IEEE Trans. Plasma Sci. **39**, 2512 (2011).
[6]C. Charles and R. W. Boswell, Plasma Sources Sci. Technol. **21**, 022002 (2012).
[7]A. Greig, C. Charles, and R. W. Boswell, "Simulations of a Capacitively Coupled Plasma Micro-Thruster using Computational Fluid Dynamics," IEEE Trans. Plasma Sci. (submitted).
[8]A. Greig, C. Charles, R. Hawkins, and R. W. Boswell, Appl. Phys. Lett. **103**, 074101 (2013).
[9]A. Agarwal, S. Rauf, and K. Collins, Plasma Sources Sci. Technol. **21**, 055012 (2012).
[10]W. B. Stein, A. A. Alexeenko, and I. Hrbud, J. Propul. Power **24**, 1007 (2008).
[11]L. Blackhall and J. Khachan, J. Phys. D: Appl. Phys. **40**, 2491 (2007).
[12]V. Guerra, E. Tatarova, F. M. Dias, and C. M. Ferreira, J. Appl. Phys. **91**, 2648 (2002).
[13]N. A. Popov, Plasma Phys. Rep. **27**, 886 (2001).
[14]M. A. Lieberman and A. J. Lichtenberg, *Principles of Plasma Discharges and Plasma Processing* (John Wiley and Sons, 2005).
[15]G. Makrinich and A. Fruchtman, Phys. Plasmas **16**, 043507 (2009).
[16]C. D. Pintassilgo, V. Guerra, O. Guaitella, and A. Rousseau, Plasma Sources Sci. Technol. **23**, 025006 (2014).
[17]D. M. Phillips, J. Phys. D: Appl. Phys. **9**, 507 (1976).
[18]R. C. Millikan and D. R. White, J. Chem. Phys. **39**, 3209 (1963).
[19]A. V. Phelps, J. Phys. Chem. Ref. Data **20**, 557 (1991).
[20]Y. Itikawa, J. Phys. Chem. Ref. Data **35**, 31 (2006).